PHYSICAL REVIEW B, VOLUME 64, 020509(R)

# Magnetic phase diagram of $Ca_{2-x}Sr_xRuO_4$ governed by structural distortions

Z. Fang[1] and K. Terakura[2,3]
[1]*JRCAT, Angstrom Technology Partnership, Central 4, 1-1-1 Higashi, Tsukuba, Ibaraki 305-0046, Japan*
[2]*JRCAT, National Institute for Advanced Industrial Science and Technology (AIST), Central 4, 1-1-1 Higashi, Tsukuba, Ibaraki 305-8562, Japan*
[3]*Research Institute for Computational Sciences (RICS), AIST, Central 2, 1-1-1 Umezono, Tsukuba, Ibaraki 305-0046, Japan*
(Received 27 February 2001; published 22 June 2001)

We constructed, by the first-principles calculations, a magnetic phase diagram of $Sr_2RuO_4$ in the space spanned by structural distortions. Our phase diagram can qualitatively explain the experimental one for $Ca_{2-x}Sr_xRuO_4$. We found that the rotation and the tilting of the $RuO_6$ octahedron are responsible for the ferro- and antiferromagnetism, respectively, while the flattening of $RuO_6$ is the key factor to stabilize those magnetic ground states. Our results imply that the magnetic and the structural instabilities in $Sr_2RuO_4$ are closely correlated cooperatively rather than competitively.

DOI: 10.1103/PhysRevB.64.020509 PACS number(s): 74.70.−b, 75.30.Kz, 71.27.+a

Both the magnetic and the structural instabilities are essential issues for the unconventional superconductivity in $Sr_2RuO_4$,[1–6] which is the only example of a noncuprate layered perovskite superconductor. It was suggested that the $Sr_2RuO_4$ is close to the ferromagnetic (FM) instability[7] with strong FM spin fluctuations, which may naturally lead to a spin-triplet *p*-wave pairing mechanism.[7–10] However, the recent observation[11] of sizable antiferromagnetic (AF) incommensurate spin fluctuation, due to the Fermi surface nesting,[12] indicates that more careful studies are needed. As for the structural aspect, it was pointed out by experiments that $Sr_2RuO_4$ is very close to the structural instability with respect to the $RuO_6$ rotation.[13] With such a situation, one may consider that three kinds of instabilities, superconducting, magnetic, and structural ones, may compete. Nevertheless, the correlation among those instabilities has not been fully discussed. It was found recently[14] that the cleaved surface of this material is reconstructed to form the $c(2\times2)$ structure which can be regarded as the frozen $RuO_6$ rotation mentioned above. Furthermore, the density-functional calculation predicts that the surface ferromagnetism is strongly stabilized by the structural reconstruction.[14] This prediction suggests that the structural and magnetic instabilities cooperate rather than compete, although the surface ferromagnetism has not been experimentally confirmed up to now.

On the other hand, the recent studies on the $Ca_{2-x}Sr_xRuO_4$ suggest strongly the cooperative feature of the structural and magnetic instabilities in the bulk. Moreover, the system shows a very rich phase diagram and provides us with an opportunity to analyze the correlation between the magnetism and the structure more extensively. Below is a brief description of the experimental observation for $Ca_{2-x}Sr_xRuO_4$ by Nakatsuji *et al.*[15] With the Ca substitution for Sr, the system is successively driven from the nonmagnetic (NM) two-dimensional (2D) Fermi liquid ($x\sim2.0$) to a nearly FM metal ($x\sim0.5$), an antiferromagnetically correlated metal ($0.2<x<0.5$), and finally an AF insulator ($x<0.2$). Since the substitution is isovalent, the dominant effects are the structural modifications due to the reduced ionic size of Ca compared with Sr. Evidence[16] has been presented by neutron scattering that the structural distortions caused by the Ca substitution correlate with the changes in the magnetic and the electronic properties.

The main aim of this communication is to study how and why the magnetism of $Ca_{2-x}Sr_xRuO_4$ is affected by structural distortions. In order to extract essential aspects, we assume that for a given crystal structure, the electronic structure is not affected by the relative content of Ca and Sr. Therefore, in the following, we study the stable magnetic phases of $Sr_2RuO_4$ for given structural distortions. Three types of structure distortions, i.e., $RuO_6$ octahedron *rotation* about the *c* axis, $RuO_6$ *tilting* around an axis parallel to the edge of octahedron basal plane and the *flattening* of $RuO_6$ along the *c* axis are identified from experiments.[16] Our phase diagram can qualitatively explain the experimental phase diagram of $Ca_{2-x}Sr_xRuO_4$, demonstrating the crucial roles of structural distortions for the tuning of electronic and magnetic properties, and further supporting our previous prediction for the surface. In particular, we found that the $RuO_6$ rotation can enhance the FM instability significantly, while the combination of tilting and rotation of $RuO_6$ is responsible for the enhancement of AF instability. Furthermore, we point out that the flattening of $RuO_6$ is a key factor to stabilize the magnetic (both FM and AF) ground states. The basic physics governing the phase diagram can be understood in terms of the strong coupling between the lattice and the magnetism through the orbital degrees of freedom. Our results strongly suggest that, in $Sr_2RuO_4$, the magnetic fluctuations can be significantly enhanced by the structural fluctuations, implying the necessity of reconsidering the coupling mechanism in the bulk superconductivity.

The calculations were performed with the first-principles plane-wave basis pseudopotential method based on the local density approximation (LDA). The validity of LDA treatment for ruthenates was demonstrated in Refs. 8 and 17. The $2p$ states of oxygen and $4d$ states of Ru are treated by the Vanderbilt ultrasoft pseudopotential,[18] while the norm-conserving scheme[19] is used for other states. The cutoff energy for the wave function expansion is 30 Ry. The *k*-point sampling of the Brillouin zone (BZ) was well checked to provide enough precision in the calculated total energies. The theoretically optimized lattice parameters $a=3.84$ Å

 

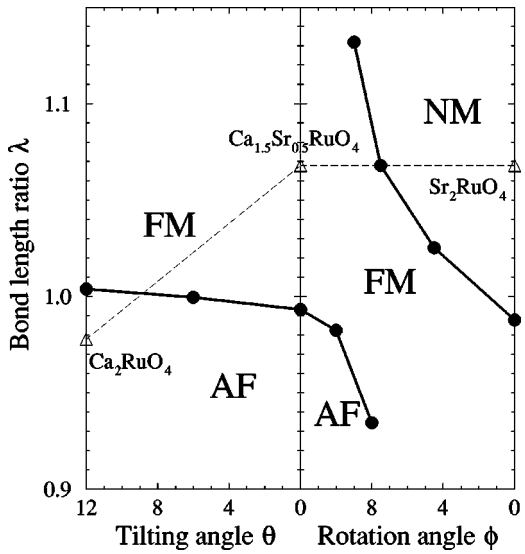


FIG. 1. The calculated magnetic phase diagram of $Sr_2RuO_4$ with structural distortions. When the tilting of $RuO_6$ octahedron is conducted, 12 degrees of $RuO_6$ rotation are reserved (see the text for a detailed description). The solid bold lines are calculated phase boundaries, while the triangles linked by a dashed line correspond to experimental data.

and $c=12.70$ Å for the bulk $Sr_2RuO_4$ are in good agreement with the experimental ones $a=3.86$ Å and $c=12.73$ Å. The degree of flattening of $RuO_6$ octahedron λ is defined by $\lambda=d_c/d_{ab}$ with $d_c$ ($d_{ab}$) denoting the Ru-O bond length along the $c$ axis (in the $ab$ plane) with the $RuO_6$ volume fixed. Rotation and tilting of $RuO_6$ octahedron are operated with the Ru-O bond lengths fixed. In order to construct the magnetic phase diagram, the lowest energy magnetic phase for each crystal structure is searched for among different (NM, FM, and AF) phases. In the present work, we focus our attention only on phases described within the $c(2\times2)$ unit cell. The soft phonon mode of $\Sigma_3$ at the zone boundary in $Sr_2RuO_4$ (Ref. 13) and the AF state of $Ca_2RuO_4$ (Ref. 20) are in this category.

Figure 1 shows the calculated phase diagram,[21] while the Table I summarizes the calculated total energies and magnetic moments for some particular points in the phase diagram. Hereafter, $\phi$ and $\theta$ denote the rotation angle and the tilting angle, respectively. The apical oxygen and the oxygen in the $ab$ plane are called O(2) and O(1), respectively. From right to left of the phase diagram, first the $RuO_6$ starts to rotate along the $c$ axis by up to 12°, and then with the 12° rotation being fixed, the $RuO_6$ starts to tilt up to 12°. The structural analysis by the neutron scattering[16] allows us to make a one-to-one correspondence between the structural changes, i.e., the horizontal axis of our phase diagram, and the doping level $x$ in $Ca_{2-x}Sr_xRuO_4$. For $x=2.0$ ($Sr_2RuO_4$), the system has $I4/mmm$ symmetry with $\phi=\theta=0°$, corresponding to the right end of our phase diagram. With reduction of $x$, $RuO_6$ starts to rotate and the symmetry is reduced to $I4_1/acd$ until $x=0.5$ ($Ca_{1.5}Sr_{0.5}RuO_4$), where $\phi=12.78°$ and $\theta=0°$ at 10 K. With further reduction of $x$, $RuO_6$ starts to tilt and the symmetry is further reduced to $Pbca$ until $x=0.0$ ($Ca_2RuO_4$), where $\phi=11.93°$ and $\theta\sim12°$ at low temperature, corresponding to the left end of our phase diagram. It was also pointed out by the experiment[16] that, from $x=2.0$ to $x=0.5$, the degree of flattening λ remains almost constant ($\sim1.07$), while from $x=0.5$ to $x=0.0$, the rotation angle $\phi$ is almost unchanged ($\sim12°$). Three representative experimental points are shown in our phase diagram by triangles. Now, the basic tendency suggested by our phase diagram is that the $RuO_6$ rotation will drive the system from a NM state to a FM state, while the subsequent tilting plus the flattening of $RuO_6$ will push the system to an AF region. This general tendency is quite consistent with the experimental results. It should be noted that the rich experimental phase diagram can be simply understood in terms of the close coupling between structural distortions and magnetism. Although the real long-range FM ordering in $Ca_{1.5}Sr_{0.5}RuO_4$ is not confirmed yet, the significant enhancement of spin susceptibility in this doping level undoubtedly implies the strengthening of FM instability. Another important aspect in our phase diagram is that the flattening of $RuO_6$ is so important not only for the AF state but also for the FM state. This suggests that *simply by uniaxial pressure, the $Sr_2RuO_4$ can be driven from the NM state to a FM state*.

TABLE I. The calculated total energies and magnetic moments for some particular points in our phase diagram.

| | NM | FM | AF |
|---|---|---|---|
| $\lambda=0.96$ | 0 meV | −40 meV | −8 meV |
| $\phi=\theta=0°$ | | $1.26\mu_B$/Ru | $0.7\mu_B$/Ru |
| $\lambda=1.07$ | 0 meV | −25 meV | |
| $\phi=12°,\ \theta=0°$ | | $0.74\mu_B$/Ru | |
| $\lambda=0.96$ | 0 meV | −100 meV | −117 meV |
| $\phi=12°,\ \theta=12°$ | | $1.13\mu_B$/Ru | $0.93\mu_B$/Ru |

The basic questions concerning our phase diagram are the following: (1) Why are the $RuO_6$ rotation and tilting correlated with the tendency to the FM and AF states? (2) Why is the $RuO_6$ flattening so important for the magnetic solutions? Before answering these questions, let us discuss the role of each $4d$ orbital in the electronic properties of $Sr_2RuO_4$, which is essential to our later discussions. The three Ru $t_{2g}$ orbitals ($d_{xy}$, $d_{yz}$, $d_{zx}$) hybridize with each other only very weakly in tetragonal $Sr_2RuO_4$. Therefore each orbital plays distinct roles. The projected density of states (DOS) shown in Fig. 2(a) indicates that the $d_{xy}$ orbital contributes dominantly to the well-known van Hove singularity (VHS) just above the Fermi level. The $\gamma$ Fermi surface has the character of $d_{xy}$. It is mostly responsible to FM spin fluctuation due to the high DOS around the Fermi level. On the other hand, $d_{yz}$ and $d_{zx}$ orbitals contribute to the $\alpha$ and $\beta$ Fermi surfaces and produce the incommensurate spin fluctuation coming from the strong nesting effect due to the quasi-one-dimensional nature of those states. The calculated bare spin susceptibility shown in Fig. 3(a) for the undistorted compound has the incommensurate peak at $\mathbf{Q}=(2\pi/3a,2\pi/3a)$, being consistent with previous calculations.[12] In real materials, the two

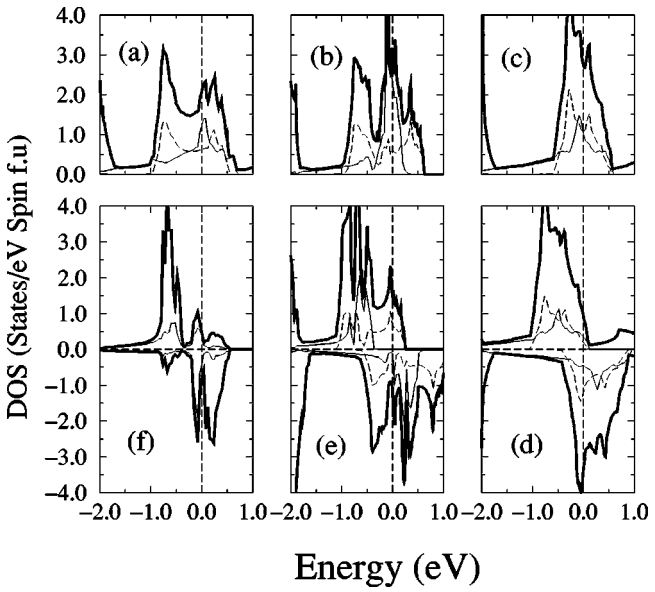


FIG. 2. The calculated electronic densities of states (DOS) for some particular points in our phase diagram, i.e., (a) $\phi=\theta=0°$, $\lambda=1.07$, NM state; (b) $\phi=12°$, $\theta=0°$, $\lambda=1.07$, NM state; (c) $\phi=\theta=0°$, $\lambda=0.96$, NM state; (d) $\phi=\theta=0°$, $\lambda=0.96$, FM state; (e) $\phi=12°$, $\theta=0°$, $\lambda=1.07$, FM state; and (f) $\phi=12°$, $\theta=12°$, $\lambda=0.96$, AF state. The bold solid lines show the total DOS [in (f), the local DOS is shown], while the thin solid and dashed lines give the projected DOS for the $d_{xy}$ and $d_{yx}$, $d_{zx}$ orbitals, respectively. Only the regions ($-2$ eV to 1 eV), where Ru-$t_{2g}$ states dominate, are shown. The Fermi levels are located at the energy zero.

factors, i.e., the FM instability due to the high DOS at the Fermi level combined with the $q$ dependent Stoner factor[8,12] and the AF instability due to the nesting effect,[12] will compete.

The $RuO_6$ rotation couples mostly with the $d_{xy}$ orbital but not with the $d_{yz}$, $d_{zx}$ orbitals because the $pd\pi$ type hybridization between the O(1)-$2p$ and the $d_{xy}$ states will be significantly reduced by the $RuO_6$ rotation, but those between the O-$2p$ and the $d_{yz}$, $d_{zx}$ states are not affected so much. The direct results of this reduced $pd\pi$ type hybridization between the O(1)-$2p$ and the $d_{xy}$ states are, first the narrowing of $d_{xy}$ band width and second the downward shift of $d_{xy}$ band, as shown in Fig. 2(b) (about 0.4 eV narrowing and 0.1 eV downward shift of $d_{xy}$ band for $\phi=12°,\lambda=1.07$). As the latter brings the VHS closer to the Fermi level, both of the two results will enhance the DOS at the Fermi level. Another effect coming from the downward shift of the $d_{xy}$ states is the population reduction in the $d_{yz}$, $d_{zx}$ states, which may shift the Fermi surface nesting vector closer to the zone boundary. However, the increase of the DOS at the Fermi level is the dominant effect and the tendency towards FM instability is enhanced by the $RuO_6$ rotation. Once tilting is additionally introduced, all of the $t_{2g}$ bands will become narrower. This will enhance the nesting effect and enhance the AF instability. The discussion so far can answer the first question.

Now let us discuss the effects of $RuO_6$ flattening. There are two factors also. First, with the flattening of $RuO_6$ octahedron, the Ru-O(1) bond length will increase, while the Ru-O(1)-Ru angle remains 180°. The increased bond length will reduce all the $pd\pi$ type hybridizations between the O(1)-$2p$ and the $d_{xy}$, $d_{yz}$, $d_{zx}$ states. Therefore, width of all the bands of three Ru-$t_{2g}$ states is reduced as shown in Fig. 2(c) (about 0.4 eV for $d_{yz,zx}$ bands and 0.3 eV for $d_{xy}$ band for $\lambda=0.96$), making the DOS at the Fermi level higher. This will favor the FM solution. Another very important results of flattening is the orbital polarization. It is obvious that the tetragonal distortion by the flattening will populate the $d_{xy}$ states and depopulate the $d_{yz}$, $d_{zx}$ states (about 0.2 eV downward shift of $d_{xy}$ band for $\lambda=0.96$). The effect is similar to the $RuO_6$ rotation. The orbital polarization due to flattening will also shift the nesting vector to the zone boundary as shown in the susceptibility calculations (Fig. 3). This will favor the commensurate AF state of the system. The net effect by rotation, tilting and flattening of the $RuO_6$ will depend on the competition among them and the phase diagram of Fig. 1 demonstrates the situation in a space spanned by those distortion modes. Figure 2(f) shows the calculated DOS for the AF state with $\phi=\theta=12°$, i.e., almost the experimental structure of $Ca_2RuO_4$. It is clear in this case that the occupied minority spin states mostly come from the $d_{xy}$ orbital due to flattening of $RuO_6$. Therefore, the strong superexchange interaction between the occupied majority-spin and unoccupied minority-spin $d_{yz}$, $d_{zx}$ orbitals will stabilize the AF ground state.[22]

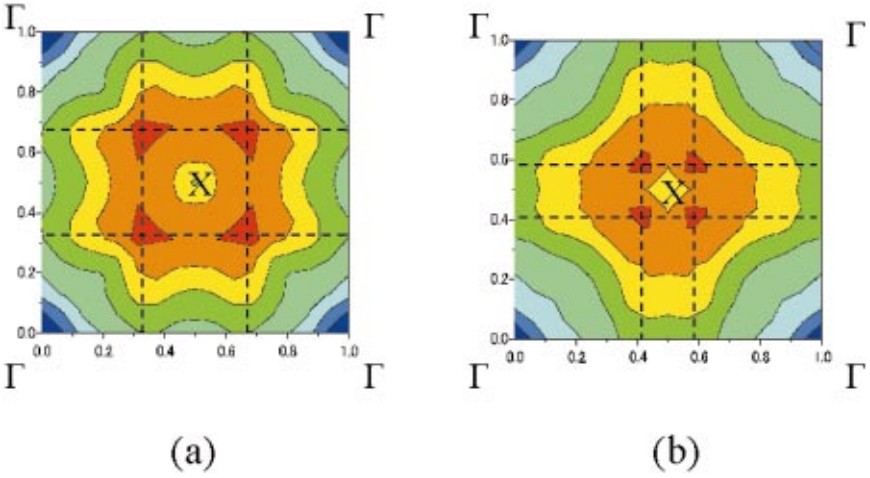


FIG. 3. (Color) A contour plot of the calculated bare spin susceptibility for (a) $\phi=\theta=0°$, $\lambda=1.07$; (b) $\phi=\theta=0°$, $\lambda=0.96$. The dashed lines are guides to the eye for the nesting vectors. The red color denotes the higher intensity.

In summary, by constructing a phase diagram of $Sr_2RuO_4$ with structural distortions, we find the strong coupling between the lattice and the magnetism. Our phase diagram can qualitatively explain the experimental phase diagram of $Ca_{2-x}Sr_xRuO_4$. We demonstrate that the $RuO_6$ rotation will enhance the FM instability in the system, while the tilting plus the flattening of $RuO_6$ make the system AF. We pointed out that the flattening of $RuO_6$ is so important not only for the AF state but also for the FM state. An important implication of our results is that the magnetic and the structural instabilities in $Sr_2RuO_4$ should be strongly correlated. The structure fluctuation and the magnetic fluctuation cooperate. Actually the phonon mode corresponding to the $RuO_6$ rotation is quite soft[13] in the bulk, and this rotation will enhance the FM instability. All these results imply the necessity of reconsidering the coupling mechanism for the unconventional superconductivity. In this context, we propose a possible way to identify experimentally the relationship between the FM fluctuation and the superconducting state. As the uniaxial compression of $Sr_2RuO_4$ will enhance the FM fluctuation without introducing the disorder, the variation of superconducting transition temperature against uniaxial compression may provide important information.

The authors thank Dr. S. Nakatsuji, Professor E.W. Plummer, Professor Y. Tokura, Dr. R. Matzdorf, and Dr. J.D. Zhang for valuable discussions and for providing us with their experimental data. One of the anthors (Z.F.) also thanks Dr. David Singh for valuable discussions. The present work was partly supported by NEDO.

[1] Y. Maeno, H. Hashimoto, K. Yoshida, S. Nishizaki, T. Fujita, J.G. Bednorz, and F. Lichtenberg, Nature (London) **372**, 532 (1994).

[2] T. Imai, A.W. Hunt, K.R. Thurber, and F.C. Chou, Phys. Rev. Lett. **81**, 3006 (1998).

[3] A.P. Mackenzie, R.K.W. Haselwimmer, A.W. Tyler, G.G. Lonzarich, Y. Mori, S. Nishizaki, and Y. Maeno, Phys. Rev. Lett. **80**, 161 (1998); **80**, 3890 (1998).

[4] G.M. Luke, Y. Fudamoto, K.M. Kojima, M.I. Larkin, J. Merrin, B. Nachumi, Y.J. Uemura, Y. Maeno, Z.Q. Mao, Y. Mori, H. Nakamura, and H. Sigrist, Nature (London) **394**, 558 (1998).

[5] T.M. Riseman, P.G. Kealey, E.M. Forgan, A.P. Mackenzie, L.M. Galvin, A.W. Tyler, S.L. Lee, C. Ager, D.M. Paul, C.M. Aegerter, R. Cubitt, Z.Q. Mao, T. Akima, and Y. Maeno, Nature (London) **396**, 242 (1998).

[6] F. Laube, G. Goll, H.v. Löhneysen, M. Fogelstrom, and F. Lichtenberg, Phys. Rev. Lett. **84**, 1595 (2000).

[7] T.M. Rice and M. Sigrist, J. Phys.: Condens. Matter **7**, L643 (1995).

[8] I.I. Mazin and D.J. Singh, Phys. Rev. Lett. **79**, 733 (1997).

[9] L. Tewordt, Phys. Rev. Lett. **83**, 1007 (1999).

[10] K. Ishida, H. Mukuda, Y. Kitaoka, K. Asayama, Z.Q. Mao, Y. Mori, and Y. Maeno, Nature (London) **396**, 658 (1998).

[11] Y. Sidis, M. Braden, P. Bourges, B. Hennion, S. NishiZaki, Y. Maeno, and Y. Mori, Phys. Rev. Lett. **83**, 3320 (1999).

[12] I.I. Mazin and D.J. Singh, Phys. Rev. Lett. **82**, 4324 (1999).

[13] M. Braden, W. Reichardt, S. Nishizaki, Y. Mori, and Y. Maeno, Phys. Rev. B **57**, 1236 (1998).

[14] R. Matzdorf, Z. Fang, X. Ismail, J. Zhang, T. Kimura, Y. Tokura, K. Terakura, and E.W. Plummer, Science **289**, 746 (2000).

[15] S. Nakatsuji and Y. Maeno, Phys. Rev. Lett. **84**, 2666 (2000); Phys. Rev. B **62**, 6458 (2000).

[16] O. Friedt, M. Braden, G. André, P. Adelmann, S. Nakatsuji, and Y. Maemo, Phys. Rev. B **63**, 174432 (2001).

[17] I.I. Mazin and D.J. Singh, Phys. Rev. B **56**, 2556 (1997).

[18] D. Vanderbilt, Phys. Rev. B **41**, 7892 (1990).

[19] N. Troullier and J.L. Martins, Phys. Rev. B **43**, 1993 (1991).

[20] M. Braden, G. André, S. Nakatsuji, and Y. Maeno, Phys. Rev. B **58**, 847 (1998).

[21] The experimental information (Ref. 16) was adopted for the structural changes in the phase diagram. However, the real alloy system $Ca_{2-x}Sr_xRuO_4$ can be treated by the virtual crystal approximation (VCA) [Z. Fang *et al.*, Phys. Rev. Lett. **84**, 3169 (2000)]. Our test calculations in the LDA for $Ca_{1.5}Sr_{0.5}RuO_4$ with experimental lattice parameters give the FM ground state with the optimized $RuO_6$ rotation angle $\phi = 9.5°$ and bond length ratio $\lambda = 1.076$.

[22] For $Ca_2RuO_4$, the generalized gradient approximation (GGA) may be better than LDA due to the narrowing of bands. However, our test calculations for $Ca_2RuO_4$ ($\phi = \theta = 12°, \lambda = 0.96$) suggested that the total energy difference between the AF and the FM solutions changes only slightly (from $-17$ meV in LDA to $-20$ meV in GGA), although a tiny gap can be obtained in GGA.